Single-electron transitions in one-dimensional native nanostructures

Journal of Physics: Conference Series **568** (2014) 052024 doi:10.1088/1742-6596/568/5/052024

Single-electron transitions in one-dimensional native nanostructures

M Reiche[1], M Kittler[2], M Schmelz[3], R Stolz[3], E Pippel[1], H Uebensee[4], M Kermann[4], and T Ortlepp[4]

[1] Max Planck Institute of Microstructure Physics, Halle, Germany
[2] BTU CS, JointLab IHP/BTU, Cottbus, Germany
[3] Leibniz Institute of Photonic Technology, Jena, Germany
[4] CIS Research Institute of Microsensorics and Photovoltaics, Erfurt, Germany

E-mail: reiche@mpi-halle.de

Abstract. Low-temperature measurements proved the existence of a two-dimensional electron gas at defined dislocation arrays in silicon. As a consequence, single-electron transitions (Coulomb blockades) are observed. It is shown that the high strain at dislocation cores modifies the band structure and results in the formation of quantum wells along dislocation lines. This causes quantization of energy levels inducing the formation of Coulomb blockades.

1. Introduction

Nanomaterials are low-dimensional materials, such as zero-dimensional quantum dots, one-dimensional nanowires, or two-dimensional sheets. The shrinkage of dimensions is expected to result in new exceeding properties related to size and quantum effects suggesting numerous new applications in electronics, optoelectronics, and other areas (e.g. [1, 2]). In recent years, silicon nanomaterials and nanostructures have been attracted extensive interest, not only for technology and device development, but also for fundamental research [3]. Here, studies of Si nanowires produced by different growth techniques were main issues [4, 5]. Preparation, handling, and packaging of individual or arrays of nanowires, however, are difficult. An alternative are dislocations. Dislocations are basic one-dimensional crystal defects. Their dimensions of a few nanometers (diameter) and lengths of more than 1 μm characterize these defects as native nanowires embedded in a perfect crystalline matrix.

The present paper deals with analysis of electronic properties of dislocations. Room temperature measurements proved already some exceptional properties such as a significant increase of the drain current of metal-oxide-semiconductor field-effect transistors (MOSFETs) if defined numbers and types of dislocations are placed in the device channel [6]. A supermetallic conductivity of dislocations was stated which is about eight orders of magnitude higher than of the surrounding silicon matrix [7]. Here, we present results of low-temperature measurements showing the presence of a two-dimensional electron gas (2DEG) at dislocation arrays. Effects related to the presence of the 2DEG (single electron transitions) are explained.

2. Sample preparation and measurement technique

A smart technique to realize reproducible arrays of dislocations is semiconductor wafer direct bonding [6, 8]. Hydrophobic bonding process initiate the formation of a two-dimensional dislocation network in the interface between both wafers. The dislocation distance in the network is well-controlled by the

misfit between both wafers. Because dislocations are crystal defects, their type depends on the crystal symmetry. Bonding of two {100}-oriented silicon wafers results, for instance, in a network of square-like meshes of screw dislocations (Burgers vector $\mathbf{b}$ = ½<110>) running parallel to both orthogonal <110> directions. To avoid interactions of dislocations with other possible defects in the bulk of wafers (point defects, etc.) silicon-on-insulator (SOI) wafers were applied. This results in dislocation networks in the center of an about 60 nm thick Si layer (device layer) electrically isolated by a buried oxide (BOX) layer from the bulk of the wafer [7].

For measurements n-channel MOSFETs (nMOSFETs) and diodes were prepared using conventional CMOS processing. The channel direction was in all cases parallel to <110>-directions, i.e. parallel to the dislocation lines (Fig.1) [6, 7]. The channel length of all devices was constant (L = 1 µm), while the channel width varied between 30 nm and 1 µm. This allows us to vary the number of dislocations in the device channel if the same dislocation network (i.e. constant dislocation spacing) is applied.

Low-temperature measurements were carried out using a cryogenic probe station ($T_{min} \cong 4$ K, Lake Shore Cryotronics) and a Physical Property Measurement System (PPMA, Model 6000, $T_{min} \cong 2$ K Quantum Design, Inc.). The latter enables also measurements in magnetic fields up to 8 Tesla. A modified Heliox VL refrigator system (Oxford Instruments) was applied for measurements down to T ≅ 300 mK. Device measurements (output and transfer characteristics of MOSFETs) were carried out using either the 4156C or B1500A Precision Semiconductor Parameter Analyzer (Agilent).

3. Results and discussion

The typical structure of a dislocation network formed by bonding of {100}-oriented Si wafers is shown in Fig. 1. The network is formed by two sets of screw dislocations parallel to orthogonal <011>-directions. Analysis at higher magnification revealed splitting of the screw dislocations into Shockley partials (Burgers vector of the type $\mathbf{b}$ = 1/6<121>) producing a stacking fault (SF) between both. The distance between both partials (or SF size) is about 6 nm [7].

Low-temperature measurements refer to Shubnikov-de Haas (SdH) oscillations if magnetic fields are applied (Fig. 2). Because SdH oscillations are proved also by setting the gate-source voltage (V_{GS}) to zero, they are induced by dislocations and not by confinement of carriers in the space charge region of

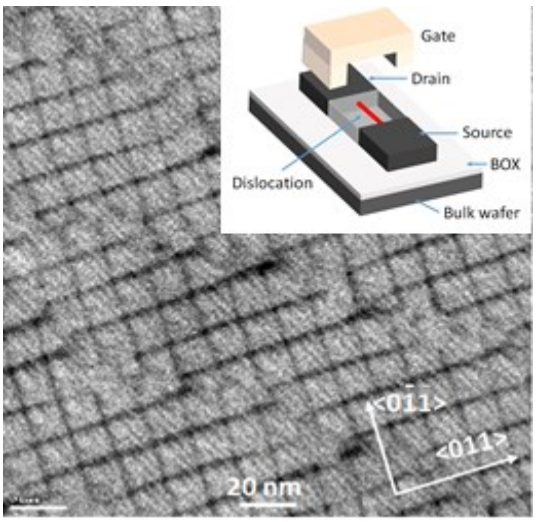

Figure 1. Transmission electron microscope (STEM) plan-view image of a screw dislocation network formed by wafer bonding of Si(100) wafers. The inset shows a schema of a MOSFET with dislocation in the channel. The gate was lifted for clarity.

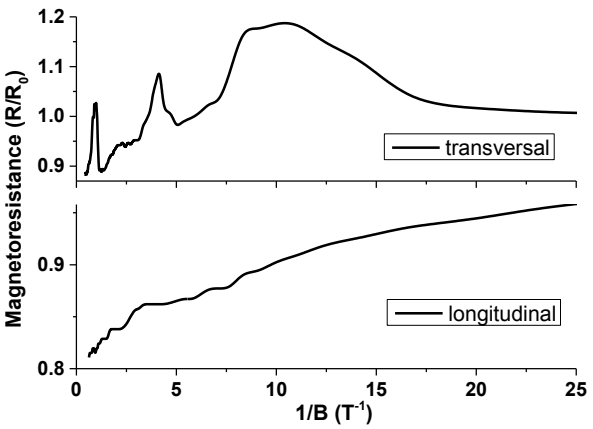

Figure 2. Transversal and longitudinal magnetoresistance vs. inverse magnetic field B. Measurement on an nMOSFET prepared on the network shown in Fig. 1 at T = 3.1 K (V_{DS} = 3V, V_{GS} = 0V).

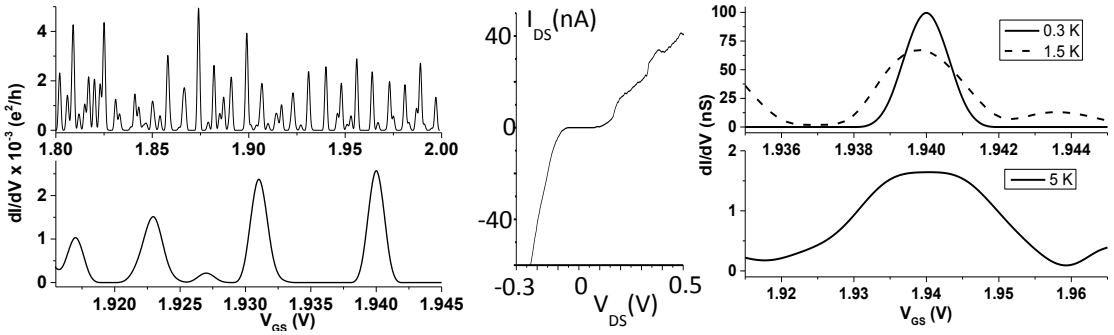

a) b) c)

Figure 3. Coulomb blockade oscillations as a function of gate-source voltage (V_{GS}) measured at T = 0.3 K and V_{DS} = 10 mV (a). The upper part shows that oscillations appear over large ranges of V_{GS}, while the lower part presents details. I_{DS}-V_{DS} characteristics at V_{GS} = 0 V and T = 0.3 K (b). Temperature dependence of the oscillations (c). Measurements at T = 0.3 K, 1.5 K, and 5 K.

MOSFETs [9, 10]. Furthermore, SdH oscillations appear also by applying a reverse bias (source-drain voltage V_{DS}). The asymmetry of the oscillations is frequently observed but different reasons are discussed (for instance [10, 11]). While dislocations represent nanowires, the asymmetry may be attributed to the fact that field-dependent oscillations are extremely sensitive to the alignment between the field and wire axis [12]. All the data suggest the presence of a two-dimensional electron gas (2DEG) on dislocations in the channel of nMOSFETs

As a consequence of the 2DEG, single electron transitions (Coulomb blockades oscillations) are observed for nMOSFETs containing dislocations in the channel. Fig. 3a shows an example of equidistant oscillations in V_{GS}, which is typical for a single-island system where each peak corresponds to the addition of one extra electron onto the island. The current-voltage (I_{DS}-V_{DS}) characteristics illustrates Fig. 3b. At T = 0.3 K a nonohmic semiconductor-like behavior with zero conductivity in the low voltage limit exists. Devices prepared on a dislocation network as in Fig. 1 were used for measurement. The period (ΔV_G) of the oscillations is about 9 mV (Fig. 3a) resulting in a gate capacitance $C_G = e/\Delta V_G$ = 18 aF. Variations of the amplitude indicate the quantum regime which can be also deduced from temperature-dependent measurements (Fig. 3c). Plots of full-width-half-maximum (FWHM) of the peak width vs. increasing temperature result in a linear dependence with a slope of the curve equal to 3.5 kT [13]. Furthermore, a conversion factor [14]

$$\alpha = \frac{5kT}{\Delta V_{FWHM}} \operatorname{arc\,cosh}\sqrt{2} \cong 0.22 \qquad (1)$$

is extracted from temperature-dependent measurements, resulting in an energy level spacing between discrete states along the wire axis $\Delta E = \alpha \cdot \Delta V_{GS}$ = 2 meV which is close to data reported from grown silicon nanowires [15].

Further information about Coulomb blockades are obtained by applying external magnetic fields. Fig. 4 shows the evolution of Coulomb blockade oscillations in dependence on the strength of magnetic fields (B) oriented perpendicular (top) and parallel to the dislocation plane (bottom). A screw dislocation network with dislocation spacing of about 10 nm was used. Without a magnetic field (B = 0 T), periodic oscillations are observed (ΔV = 54 mV). Applying a magnetic field perpendicular to the dislocation plane does not change the oscillation distance and peak width for both sets of orthogonal dislocations. Higher bias conditions, however, decrease the amplitude of the oscillations. On the other hand, an increase of the amplitude is found for Coulomb blockade oscillations proved by measurements of devices containing the orthogonal set of screw dislocations of the network. This cannot be explained by an increase of diffusion-controlled transport to the dominant tunneling at low bias conditions. Instead, a different modification of the spatial extent of the ground state wave function by the magnetic field is assumed which causes changes of the level width and density, resp. [16].

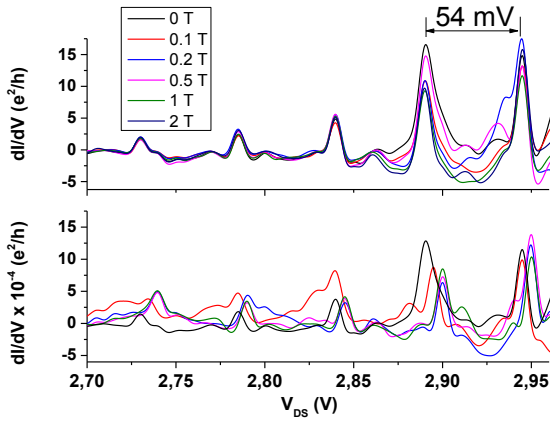

Figure 4. Evolution of Coulomb blockade oscillations with magnetic field perpendicular (top) and parallel to the dislocation plane (bottom).The strength of the magnetic field is indicated in the figure. Measurements at T = 3.1 K.

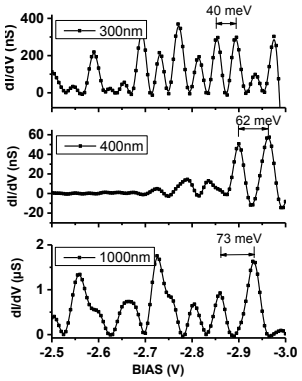

Figure 5. Dependence of the Coulomb blockade oscillations on the number of parallel dislocations. Increasing the channel width (indicated in figures) increases the number of dislocations. The same dislocation network is used. Measurements at T = 4.3 K.

Characteristic changes of the oscillations appear by applying a magnetic field parallel to the dislocation plane (Fig. 4, bottom). Increasing B results not only in shifts of the oscillation peaks, but also in their splitting. The shifts of the oscillation peaks increase for $B \leq 0.5$ T and are constant for higher values of B. The maximum shift is about 10 mV but is not constant for all peaks. Similar values of the shifts of oscillation peaks have been also measured for the orthogonal set of dislocations. Furthermore, peak splitting is observed with varying magnetic field. Both, the peak shift and peak splitting are caused by the fact that the chemical potential of a quantum dot in a parallel magnetic field has two additional terms [17], the diamagnetic shift ($\gamma_N B_{\|}^2$) describing the shift of the energy levels due to a squeezing of the wave functions, and the Zeeman splitting

$$\Delta E_{Zeeman} = \pm \frac{1}{2} g^* \mu_B B_{\|} \quad . \tag{2}$$

Here , γ_N denotes the effective diamagnetic factor, g^* the effective g factor, and μ_B the Bohr magneton. While the diamagnetic shift is proportional to $B_{\|}^2$, the Zeeman splitting is linear in $B_{||}$.

The periodicity of the Coulomb blockade oscillations depends not only on the dislocation type but also on the number of parallel dislocations in the device channel. Fig. 5 shows the oscillations of three devices prepared on the same dislocation network. The width of the device channel was varied from 300 nm to 1000 nm, which means an increase of the number of dislocations by more than a factor of three. Note that the dislocation spacing is the same in all cases. At the smallest channel width (300 nm, corresponding to about 15 dislocations), the period of the oscillations is 40 mV and increases by a factor of 1.5 to 62 mV if the channel width increases to 400 nm (i.e. about 26 dislocations). A further increase of the channel width to 1000 nm (corresponding to about 67 dislocations) increases the period to 73 mV. Increasing the number of dislocations increases not only the period of the Coulomb blockade oscillations but also their amplitude. Both refer to interactions between the quantum dots on different dislocations.

The formation of a 2DEG along individual dislocations lines is a direct consequence of the high strain level on the dislocation core exceeding 10 %, or more [7]. In the case of a screw dislocation, discussed here, the strain is tensile. Such high strain levels result in dramatic changes of the electronic band structure. Band structure calculations using an 8-band-**k**·**p**-model and an empirical $sp^3d^5s^*$ tight binding model clearly showed that the effective electron mass shrinks and the band gap at the Γ-point is reduced at strain levels of $\varepsilon \geq 10$ % [18]. The band gap at the Γ-point reaches the same value as for

the indirect band gap between the Γ- and Δ-point. This means that Si changes into a direct semiconductor and the dislocation forms a quantum wire structure where electrons are confined in the direction of the wire axis.

4. Conclusions

Dislocations are one-dimensional crystal defects in a perfect crystalline matrix. Their properties characterize the defects as one-dimensional nanowires. In particular, the strain in the dislocation core causes changes of the band structure resulting in the formation of a quantum well along the dislocation line. Within the well, quantization of energy levels exists where the energy levels depend on the width (or diameter) of a dislocation. A consequence of the quantum well is the formation of a 2DEG for two-dimensional dislocation networks and the quantization of energy levels induces the formation of Coulomb blockades. The measured distances of Coulomb blockades corresponds to the lowest energy levels if widths of the blockades of about 5 nm are assumed in calculations [18].

References

[1.] Cao G and Wang Y 2011 *Nanostructures and nanomaterials - synthesis, properties, and applications*. 2nd ed (Singapore: World Scientific Publ.).
[2.] Zhang R-Q 2014 *Growth mechanisms and novel properties of silicon nanostructures from quantum-mechanical calculations* (Heidelberg: Springer).
[3.] Koshida N (editor) 2009 *Device applications of silicon nanocrystals and nanostructures* (New York: Springer).
[4.] Huang Y and Tu K-N (editors) 2013 *Silicon and silicide nanowires* (Boca Raton: CRC Press).
[5.] Schmidt V, Wittemann JV, Senz S and Gösele U 2009 Adv Mater **21** 2681.
[6.] Reiche M, Kittler M, Scholz R, Hähnel A and Arguirov T 2011 J Phys Conf Ser **281** 012017.
[7.] Reiche M, Kittler M, Erfurth W, Pippel E, Sklarek K, Blumtritt H, Haehnel A and Uebensee H 2014 J Appl Phys **115** 194303.
[8.] Reiche M and Gösele U 2012 Direct Wafer Bonding *Handbook of Wafer Bonding* eds P Ramm, JJ-Q Lu, MMV Taklo (Weinheim: Wiley-VCH) pp 81-100.
[9.] Kravchenko SV, Shashkin AA, Bloore DA and Klapwijk TM 2000 Solid State Commun **116** 495.
[10.] Haug RJ, von Klitzing K and Ploog K 1987 Phys Rev B **35** 5933.
[11.] Griffin N, Dunford RB, Pepper M, Robbins DJ, Churchill AC and Leong WY 2000 J Phys: Condens Matter **12** 1811-8.
[12.] Shim W, Ham J, Kim J and Lee W 2009 Appl Phys Lett **95** 232107.
[13.] Kouwenhoven LP, Marcus CM, McEuen PL, Tarucha S, Westervelt RM and Wingreen NS 1997 Electron transport in quantum dots *Mesoscopic electron transport* eds LL Sohn, LP Kouwenhoven, G Schön (Dordrecht: Kluwer).
[14.] Tilke AT, Simmel FC, Blick RH, Lorenz H and Kotthaus JP 2001 Progr Quant Electron **25** 97.
[15.] Zhong Z, Fang Y, Lu W and Lieber CM 2005 Nano Letters **5** 1143.
[16.] Aravind K, Lin MC, Ho IL, Wu CSK, W., Kuan CH, Chang-Liao KS and Chen CD 2012 J Nanosc Nanotechnol **12** 2509.
[17.] Rahimi-Iman A, Schneider C, Fischer J, Holzinger S, Amthor M, Höfling S, Reitzenstein S, Worschech L, Kamp M and Forchel A 2011 Phys Rev B **34** 165325.
[18.] Reiche M, Kittler M, Uebensee H, Pippel E, Haehnel A and Birner S 2014 submitted to Phys Rev B.